Applied Catalysis B: Environmental 87 (2009) 1–8

Contents lists available at ScienceDirect

Applied Catalysis B: Environmental

journal homepage: www.elsevier.com/locate/apcatb

Preparation of black sand-based magnetic photocatalysts for photocatalytic oxidation of aqueous phenol

Mingliang Luo [a,b,*], Derek Bowden [b], Peter Brimblecombe [b]

[a] School of Chemistry, Sichuan University, Chengdu, Sichuan, 610064, PR China
[b] School of Environmental Sciences, University of East Anglia, Norwich, Norfolk, NR4 7TJ, United Kingdom

ARTICLE INFO

Article history:
Received 10 May 2008
Received in revised form 29 August 2008
Accepted 8 September 2008
Available online 16 September 2008

Keywords:
Magnetic photocatalyst
Black sand
Titanium dioxide
Phenol
Silica coating

ABSTRACT

A natural magnetic material, black sand, was used as cores to prepare a magnetic photocatalyst, which can be recovered using an external magnetic field. A surfactant-involved scheme was proposed to deposit a rough silica layer on the surface of black sand, which otherwise could not be coated with silica through a conventional scheme involving Stöber process. Titanium dioxide (TiO_2) was deposited on the surface of the silica–black sand (Si/BS) through an impregnation process and a direct deposition process. The catalytic property of the resultant photocatalyst (Ti/Si/BS) was evaluated using the oxidation of aqueous phenol and exhibited less reactivity than Degussa P25 TiO_2. The phenol removal efficiency showed a pH dependence, which was ascribed to pH effect on (a) the formation of $^{\bullet}OH$ and (b) the electrostatic interaction between the photocatalyst and the substrate. The prepared photocatalyst is reusable despite slight deactivation caused by the mechanical loss of TiO_2.

1. Introduction

Titanium dioxide (TiO_2) has become the most successful photocatalyst and intensively investigated [1] since Fujishima and Honda's discovery of the photolysis of water by titanium compounds in 1972 [2]. In the field of environmental remediation, the TiO_2 photocatalytic process is economically favorable since it is able to exploit sunlight and air to destroy pollutants. The TiO_2 photocatalyst is often used in slurry form, composed of ultra-fine particles, such as the commercial product Degussa P25. However ultra-fine particles often cause recycling problems, after use in water, because they do not easily sediment. Hence developing an appropriate form of TiO_2 that favours recovery has become an objective in this field. A popular method is to immobilize TiO_2 in film form on some inert substances [3–6]. However, this is suggested as less accessible to reactants in water and thus less efficient than a dispersed TiO_2 slurry [7].

Recently photocatalysts on a magnetic support have become prominent to address this issue [8–16]. They are a composite comprising a TiO_2 shell and a magnetic core that makes them recoverable using an external magnetic field. Additionally, their particle form circumvents the drawback of the lack of accessibility of TiO_2 films to the reactants. A simple method of preparing a magnetic TiO_2 photocatalyst involves depositing TiO_2 on magnetic iron oxide cores. However, such arrangement will bring about photo-dissolution of iron during photoreaction [13,14], as a result of the charge transfer between TiO_2 and iron oxide. Therefore it is necessary to have an insulating layer, typically a silica layer, between the magnetic core and the surface TiO_2 to prevent this charge transfer. The development of such titania–silica–magnetite composites begins with the preparation of the core materials, which are often nanosized iron oxide particles made in the laboratory through hydrolysis and precipitation of iron salts [8,10–14,17]. The core particles are then coated with a silica layer usually through a sol–gel scheme involving the Stöber process. Afterwards TiO_2 is deposited on the silica–magnetite composite to obtain the magnetic photocatalyst.

In terms of the magnetic recoverability, it is believed that the finer the magnetic particles, the weaker the interaction with the external magnetic field and the more difficult it becomes to recover the catalyst from water [18]. With few exceptions [9,16], most magnetic photocatalysts that comprise fine magnetic core particles are recovered by centrifugation in the laboratory despite the assumption that they are magnetically recoverable [8,10–15]. Thus, it is of practical interest to investigate the use of coarse materials as magnetic cores. Here, black sand (BS), a natural magnetic material collected on New Zealand beach, was used as the magnetic core. The size of black sand ranges from 100 to 200 μm and can easily be tailored by grinding process to meet

* Corresponding author.
E-mail address: luoml@163.com (M. Luo).

0926-3373/$ – see front matter © 2008 Elsevier B.V. All rights reserved.
doi:10.1016/j.apcatb.2008.09.002

the size requirements. Apart from its controllable size, this natural material is also preferred in economic aspect to the laboratory-made nanosized iron oxide particles.

During the preparation process in this research, black sand was first crushed in a ball mill to reach an average size around 10 μm, yet still able to produce sensible interaction with the external magnetic field. The crushed black sand was then coated with a silica layer through a modified coating scheme involving surfactant hexadecyl trimethyl ammonium chloride (C_{16}TACl). Titanium dioxide was subsequently deposited on the silica-coated black sand (Si/BS) to obtain the magnetic photocatalyst (Ti/Si/BS), whose reactivity was examined using the photocatalytic oxidation of aqueous phenol, a representative pollutant.

2. Experimental

2.1. Preparation of Si/BS composite

The crushed black sand particles (0.3 g) were dispersed in purified water (200 ml, Neptune Purite) containing C_{16}TACl (1.6 ml, ~25 wt%, Fluka) and tetraethyloxysilane (3.0 ml, purum, Fluka). After stirring for a short while (~2 min) with an overhead stirrer, the mixture was agitated with ultra-sonication (Decon) for 20 min to improve the dispersion of particles. Ammonium hydroxide (1.0 ml, ~28 wt%, Acros) was then added drop-wise into the mixture. After a 2-h period of continuous stirring, the precipitate was separated with centrifugation and washed with purified water. Finally the precipitate was dried overnight at 100 °C prior to calcination for 2 h at 500 °C.

2.2. Preparation of Ti/Si/BS photocatalyst

2.2.1. Through an impregnation procedure

Titanium tetra-isopropoxide (1.5 ml, purum, Fluka) was dissolved in isopropanol (40.0 ml, analytical reagent, Fisher Scientific). Pre-dried Si/BS particles (0.2 g) were dispersed in the solution and agitated with ultra-sonication for 30 min. Then the mixture was stirred for 5 h in a beaker placed in fume cupboard, which in most cases caused the evaporation of all the solvent. The mixture was heated at 80 °C for 3 h and then calcined at different temperatures for 3 h. The final product was crushed gently in a crucible and was designated Ti/Si/BS-A.

2.2.2. Through a direct deposition procedure

A modified direct deposition procedure was developed, including preparation of TiO_2 colloidal solution in acidified water [19] and deposition of TiO_2 on Si/BS particles.

Step 1: Preparation of TiO_2 colloidal solution.

Isopropanol (10.0 ml) was mixed with purified water (200 ml) and the pH of the mixture was then adjusted to 1.5 with HCl. Titanium tetra-isopropoxide (1.0 ml) dissolved in isopropanol (10.0 ml) was slowly dripped into the above mixture with vigorous stirring. Initially white flocs formed with the precipitation of titanium dioxide; after overnight stirring the mixture became transparent, however. The transparent colloidal solution may be stable for several days in room temperature and for months in a refrigerator at −4 °C.

Step 2: Deposition of TiO_2 on Si/BS particles

Silica-coated black sand particles (0.2 g) were dispersed in TiO_2 colloidal solution (50 ml) by stirring. The mixture was then agitated with ultra-sonication for 20 min. Afterwards the pH of the mixture was adjusted to ~3.0 with HCl and the mixture was immediately heated on a hotplate to raise the temperature to 90 °C quickly. The mixture was kept at this temperature for 2 h with stirring, then repeatedly centrifuged and washed with purified water. Finally the product was dried overnight at 80 °C and was designated Ti/Si/BS-B. In order to evaluate the effect of heat treatment on the crystallographic transformation of TiO_2, some samples were calcined at different temperatures.

2.3. Separation of Ti/Si/BS photocatalyst

The objective of this research is to prepare a magnetic photocatalyst, but there were probably three forms of TiO_2 generated during its deposition, i.e., the separated TiO_2 particles, the loosely adsorbed TiO_2 particles on the Si/BS particles and the tightly bound TiO_2 components on the Si/BS particles. As a photocatalyst, the first and the second (whose TiO_2 components would easily come off the core particles) are effectively no different to ordinary pure TiO_2 particles. Only the third is desired with respect to the objective here and needs separation. This need was mentioned by only few reports [9,20]. Here a separation process is proposed as follows.

The synthesized particles (approximately 1.0 g) were dispersed by stirring vigorously (800 rpm) for 20 min in a beaker containing purified water (75 ml). A handheld magnetic stirrer bar was used to attract and collect the magnetic portion from the slurry (Fig. 1). The collected particles were then washed and separated a further three times. The particles finally collected represented the desired Ti/Si/BS composites. It should be highlighted that, due to the weak magnetic force produced by the stir bar, there was some loss of very fine Ti/Si/BS particles.

2.4. Characterization of Ti/Si/BS photocatalysts

Scanning electron microscopy combined with energy dispersive spectrometry (SEM–EDS, JSM 5900 LV) was used to obtain morphology and semi-quantitative elemental composition of the particle surface. An inductively couple plasma-mass spectrometer (ICP-MS, Thermal X7) combined with a laser ablation sampler was also employed to determine the contents of Fe, Si and Ti on the particle surface. X-ray diffraction (XRD, Thermal ARL) was utilized to analyze the crystallography of surface titanium dioxide. Nitrogen adsorption at 77 K was performed (AutoSorp ZXF-6, PR China) to measure the specific surface area of the particle samples according to Brunauer–Emmett–Teller (BET) equation.

Fig. 1. Attraction and collection of Ti/Si/BS particles using a handheld magnetic stirrer bar.

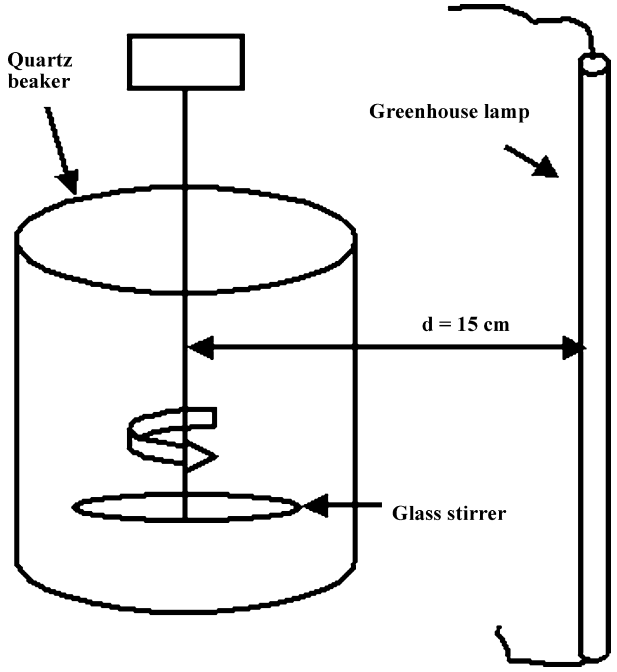

Fig. 2. Apparatus for the photocatalytic experiments.

2.5. Photocatalytic oxidation of phenol

The experimental apparatus was shown in Fig. 2. Phenol solution (75 ml) with concentration of 20 mg L^{-1} was prepared in a quartz beaker and the Ti/Si/BS photocatalyst (0.2 g) was dispersed in the solution with stirring. A greenhouse lamp (M7, 400W, Cryselco Ltd., UK; emission spectrum of the lamp was given in Fig. 3) was used to irradiate the quartz beaker for the photocatalytic oxidation of phenol. During the reaction, aliquots of the solution were removed into a sample tube at preset time intervals and filtered with a syringe filter (0.22 μm, Millipore). The filtrate (2.5 ml) was then transferred into a 25-ml flask, followed by addition of amounted NH_3H_2O–NH_4Cl buffer (pH 10), 4-aminoantipyrine solution and $K_3Fe(CN)_6$ solution to determine the concentration of phenol with a UV/vis spectrometer (Lambda 25, PerkinElmer) [21].

As a comparison, Degussa P25 TiO_2 powder was also used for the photocatalytic oxidation of phenol. The applied dosage of P25 TiO_2 powder was 0.1 g in 75 ml of phenol solution, close to the optimal dosage 1 kg m^{-3} [22]. The experimental procedure was similar to the above except the removed aliquots were centrifuged, not filtered, for the subsequent determination process because P25 TiO_2 particles are fine enough to penetrate the filters.

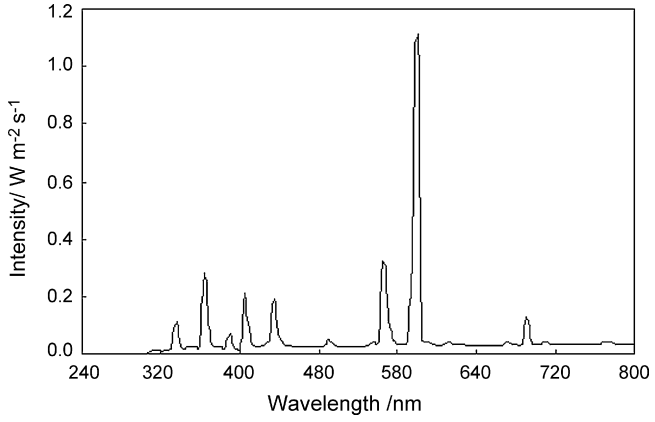

Fig. 3. Emission spectrum of the greenhouse lamp.

2.6. Repeat use of Ti/Si/BS photocatalysts

The Ti/Si/BS photocatalysts were recovered using a handheld magnetic stir bar after use through the same scheme as described above. The recovered particles were washed with copious pure water and then used again for photoreaction. Each time a fresh phenol solution with identical concentration (75 ml at 20 mg L^{-1}) was used for the photoreaction.

3. Results and discussion

3.1. Coating black sand with a rough silica layer

The morphologies of black sand, crushed black sand and Si/BS are shown in Fig. 4. On the surface of Si/BS particles, a rough silica layer is in evidence (Fig. 4c), consisting of silica spheres with size around 100 nm (Fig. 4e). The contents of Fe, Si and Ti of the related materials are shown in Table 1. A comparison of black sand and Si/BS shows that the silica coating resulted in substantial increase in the silicon percentage and concurrent decrease in the percentages of both iron and titanium. The deposition of the rough silica layer also caused a drastic increase in the surface area as seen in Table 1.

The silica coating scheme used in this research differs from the conventional sol–gel scheme using the Stöber process. The Stöber process itself is long renowned for synthesis of silica spheres with size ranges from tens of nanometer to sub-micrometer [23–30]. The conventional sol–gel coating scheme is performed in an alcohol medium and often applied to the nanosized magnetite particles while its application to larger particles (e.g., size > 10 μm) is rare. There was an attempt in this research to coat black sand through the conventional coating scheme, but it was unsuccessful, possibly because of the weak interaction between the nanosized silica sphere and the far larger black sand particles. Thus a modified coating scheme involving surfactant $C_{16}TACl$ was adopted to achieve the deposition of silica on black sand particles. This modified coating scheme was carried out in aqueous medium and achieved a rough silica layer covering on the particles. This surfactant mediated coating scheme presumably proceeds through (a) a silica–surfactant self-assembly mechanism to generate silica spheres [31,32] and subsequently (b) surfactant-enhanced interfacial attraction [33,34] which bonds the silica spheres and black sand particles.

3.2. Deposition of titanium dioxide on Si/BS particles

The morphology of Ti/Si/BS-A and B, though with TiO_2 deposited on the surface, showed no obvious difference from that of Si/BS (the image of Ti/Si/BS-A was presented in Fig. 4). The deposition of titanium dioxide on the surface is suggested by the drastic increase of titanium percentage and the decrease of those of silicon and iron, by comparing Si/BS to Ti/Si/BS-A or B in Table 1. According to the ICP-MS results, the amount of Ti deposited on Ti/Si/BS-A and B particles are estimated around 5–7 wt% by comparing Ti percentages of Ti/Si/BS-A or B, Si/BS and black sand. Additionally Ti/Si/BS-A exhibits a higher iron percentage (18.55 wt%) than Ti/Si/BS-B (9.12 wt%). The surface areas of both Ti/Si/BS-A and Ti/Si/BS-B decreased when compared to that of Si/BS. Particularly the bigger drop in the surface area related to Ti/Si/BS-A is ascribed to the heat treatment that induced the formation of anatase TiO_2 in the impregnation procedure.

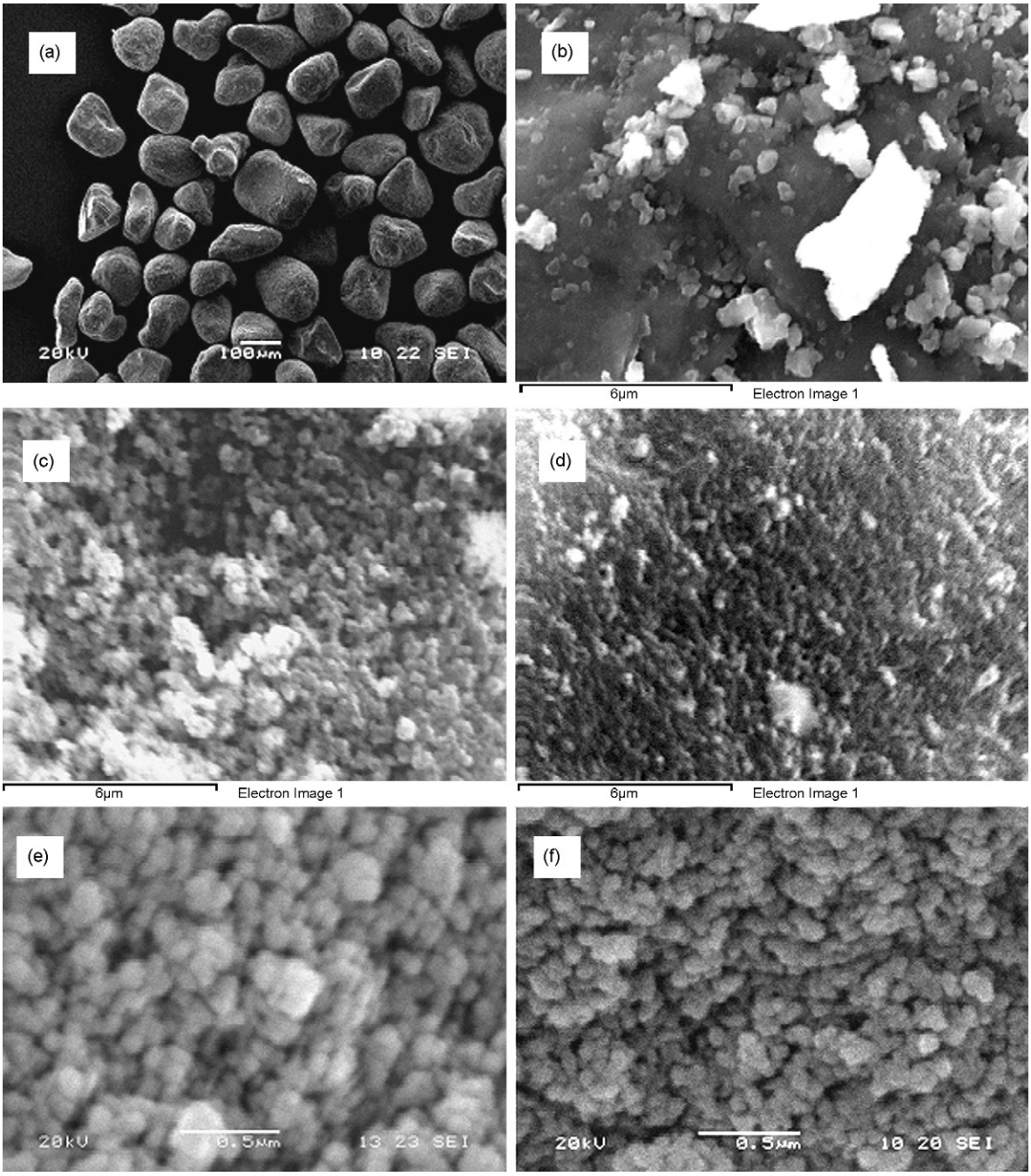

Fig. 4. SEM micrographs of black sand (a), crushed black sand (b), Si/BS (c), Ti/Si/BS-A (d), Si/BS (e) and Ti/Si/BS-A (f).

Table 1
TiO_2 crystallite size, surface area and content (in wt%) of Fe, Si and Ti of the catalysts.

	Anatase crystallite size (nm)	Surface area ($m^2\ g^{-1}$)	Obtained with SEM–EDS			Obtained with ICP-MS		
			Fe	Si	Ti	Fe	Si	Ti
Degussa P25	21	50[a]	–	–	–	–	–	–
Black sand	–	1.785	43.13	0.73	7.40	27.94	1.54	2.54
Si/BS	–	166.9	12.84	10.84	1.98	5.06	10.48	0.57
Ti/Si/BS-A	10	80	1.54	2.24	11.26	18.55	11.00	7.50
Ti/Si/BS-B	6	123.7	0.72	1.54	11.85	9.12	20.64	7.06
Ti/Si/BS-A[4]	–	–	1.75	3.45	13.91	–	–	–
Ti/Si/BS-A[6]	–	–	1.63	2.31	12.90	–	–	–
Ti/Si/BS-A[8]	–	–	2.05	1.23	7.15	–	–	–

Note: the superscript numbers following Ti/Si/BS-A indicate the repeat time of use.
[a] As reported in the specification of the product.

Regarding the deposition mechanism, the impregnation procedure was suggested to consist of two steps: (a) chemisorption of titanium alkoxide onto the surface silanol group (Si–OH) and (b) subsequent hydrolysis of the titanium alkoxide in air after evaporation of solvent [35]. The direct deposition process probably proceeded through heterocoagulation between TiO_2 colloidal particles and the Si/BS surface [11,12,36]. This depends on pH conditions and isoelectric points (IEPs) of both substances. Knowing the IEPs for TiO_2 and SiO_2 are ~6.0 and ~2.0, respectively, this research used pH 3.0 to promote heterocoagulation, also in line with that used elsewhere [12]. During the process of direct deposition, a small amount of iron probably dissolved from Si/BS particles when the particles were placed in the TiO_2 colloidal solution at pH ~1.5 for a short while. This causes a lower bulk iron content in Ti/Si/BS-B than in Ti/Si/BS-A as shown in Table 1 (9.12 wt% versus 18.55 wt%).

The crystalline transformation of deposited TiO_2 is evaluated by XRD analysis as shown in Fig. 5, where black sand, Si/BS and Degussa P25 TiO_2 are presented for comparison. As far as the impregnation process is concerned, the unheated Ti/Si/BS-A particles exhibited amorphous TiO_2 deposition. Heat treatment with temperatures ranging from 350 to 650 °C transformed the TiO_2 into the desired anatase phase. At 450 °C the indicative peak (25.4°) for anatase phase already became prominent. Given the detrimental effects of high temperature treatments on the catalysts, e.g., decrease of surface area and demagnetization of core materials, the modest temperature 450 °C was adopted hereafter, near the temperatures often used by other researchers [8,11,37,38]. In contrast, the direct deposition process achieved anatase TiO_2 at a lower temperature (90 °C), agreeing well with the observation elsewhere [39]. The indicative peak for anatase TiO_2 deposited on the unheated Ti/Si/BS-B particles is broader but recognizable, and became more prominent after heat treatment at 350, 450 and 550 °C. The XRD analysis also evidenced the minor presence of rutile TiO_2 ($2\theta = 27.4°$) in the Ti/Si/BS-B samples. The crystallite sizes of anatase TiO_2 deposited on both Ti/Si/BS composites are worked out according to Scherrer equation, which are smaller than that of P25 TiO_2 (Table 1). Compared to the impregnation process, the advantage of the direct deposition process is apparently that it is able to avoid the unfavorable heat treatment to obtain an anatase TiO_2.

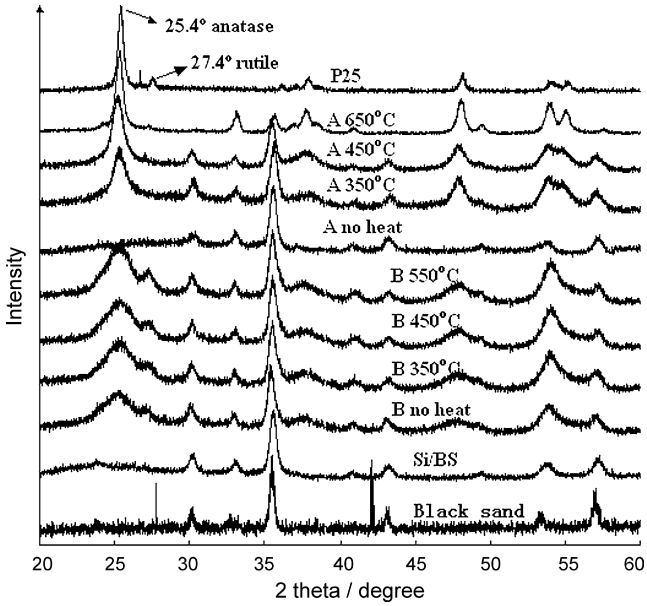

Fig. 5. XRD spectra of Ti/Si/BS-A and Ti/Si/BS-B after calcination at different temperatures.

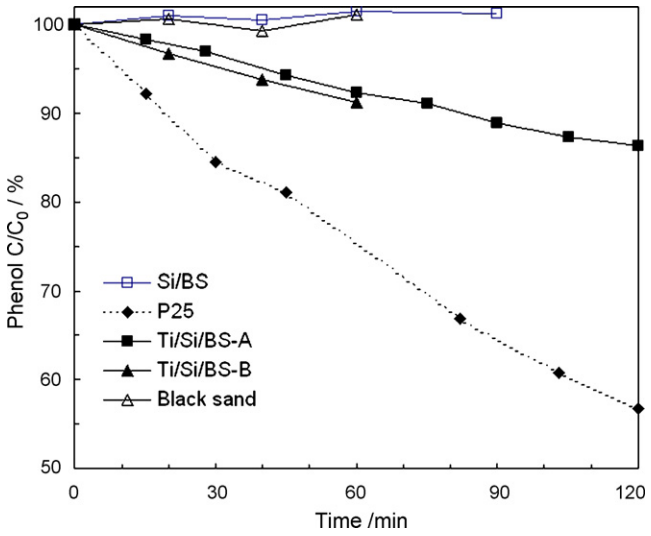

Fig. 6. Photocatalytic oxidation of phenol with different particles.

3.3. Performance of Ti/Si/BS composites in the photocatalytic oxidation of phenol

Fig. 6 shows the catalytic performances of different materials with respect to the photocatalytic oxidation of phenol. Generally black sand and the Si/BS composite were not active photocatalysts. Both Ti/Si/BS-A and Ti/Si/BS-B were able to promote the photocatalytic oxidation of phenol, although they were less efficient than Degussa P25 TiO_2. The decreases in phenol concentrations are approximately linear with respect to the observed time period. Under identical experimental conditions, the phenol removal efficiencies were ~8.0, ~9.0 and ~24.0 wt% after 1-h reaction period for Ti/Si/BS-A, Ti/Si/BS-B and Degussa P25 TiO_2, respectively. Adsorption tests suggested no appreciable adsorption (<1 wt%) of phenol occurred on the surface of the Ti/Si/BS particles. The adsorption of phenol by Degussa P25 TiO_2 was also negligible [22,37]. The removal efficiency of phenol was influenced by the

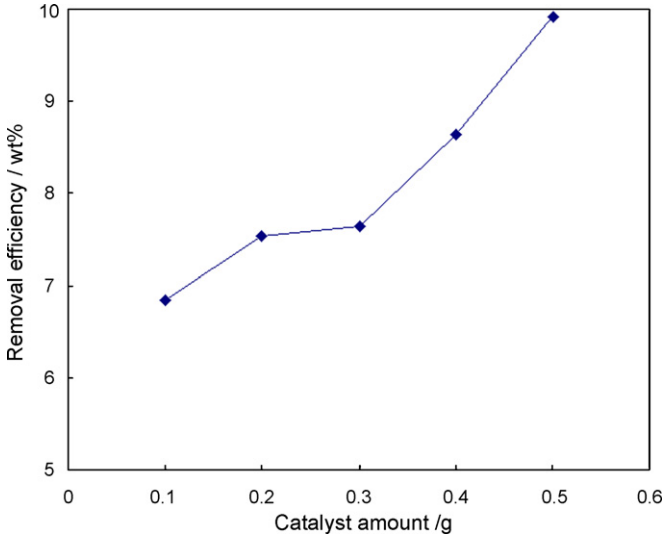

Fig. 7. Effect of catalyst amount on the phenol removal efficiency after 1-h photoreaction.

amount of photocatalyst, as shown in Fig. 7 (only Ti/Si/BS-A composite was evaluated). It is proportional to the amount of suspended catalyst.

Normally Degussa P25 TiO_2, a commercial product with consistent properties, is used as a benchmark to assess the efficiency of a photocatalytic process. The Ti/Si/BS particles exhibit ~1/3 as efficient as P25 TiO_2. Lower efficiencies were also observed with other similar supported-TiO_2 photocatalysts [8,11,16,20,37]. In this research it is related to the small loading of TiO_2 on the Ti/Si/BS composite. According to the ICP-MS analysis in Table 1, 0.2 g Ti/Si/BS-A and B particles used for the photocatalytic experiments contributed effectively 0.016 and 0.015 g of TiO_2, respectively (estimated by comparison to black sand), which account only a fraction of the amount (0.1 g) of P25 TiO_2 used in the comparison experiment. It has been reported that the efficiency increased with increasing presence of TiO_2 under a threshold value [40–42]. One way to increase the presence of TiO_2 is to increase the amount of Ti/Si/BS catalyst, the effect of which has already been observed in Fig. 7 where the rate of photoreaction is proportional to the amount of the photocatalyst. Alternatively, it was also suggested that a better photoreactivity could be obtained by raising the percentage of TiO_2 of the catalyst through repeated deposition process [16,42].

The kinetic rates normalized per mass of TiO_2 were 1.06, 1.28 and 0.51 mmol L^{-1} h^{-1} g^{-1} TiO_2 for Ti/Si/BS-A, Ti/Si/BS-B and P25, respectively, indicating that the magnetic photocatalyst was about twice as efficient as the P25 catalyst on a TiO_2 weight-to-weight basis. The photoreactivity of pure TiO_2 is often related to its texture properties such as the amount of anatase, surface area and crystallite size [38,43,44]. In this work, both Ti/Si/BS-A and Ti/Si/BS-B were coated mainly with anatase TiO_2 whose crystallite sizes are smaller than that of P25 TiO_2 (Table 1). This seems not supporting the higher photoreactivity as it was found that the photoreactivity of anatase TiO_2 was proportional to the crystallite size [43]. The higher photoreactivity of deposited TiO_2 thus probably arose from the silica-induced properties on the composite surface. For example, the silica coating can often produce a large surface area and change the surface charge of the catalyst, and hence favor the access of reactants to the catalytic sites [42,45,46].

3.4. pH dependence of photoreduction rate of phenol

The catalytic reactivity of the Ti/Si/BS photocatalyst exhibits a pH dependence as shown in Fig. 6 (the solid line), where the phenol removal efficiency peaked around pH 7.0–8.0. The pH dependence has previously been reported [40,47–52], which typically follows a trend where the rate increases or decreases and then becomes constant at a certain pH value. This is often related to one of the two factors: (a) the pH effect on the formation of hydroxyl radicals or (b) the pH effect on the electrostatic interaction between TiO_2 and substrates. Here, the pH dependence of rate showed a more complicated trend (the peak) that could be attributed to both factors acting together.

To elucidate the mechanism of pH effect, a simple model of this oxidation reaction is proposed as follows. The TiO_2-mediated photocatalytic oxidation is assumed to be mainly promoted by hydroxyl radicals on the surface of the catalyst particles. In terms of phenol, both the non-ionized molecular (HPh) and phenoxide anion (Ph^-) are possible reactants. This is determined by their electrostatic interaction with the charged catalyst surface, which is probably controlled by the dissociation of hydrous SiO_2. The isoelectric point of SiO_2 is around 2.0 [12,53], thus under pH (>2.0) used in the experiments, the hydrous SiO_2 is negatively charged and would expel the phenoxide anion. Consequently a surface oxidation between hydroxyl radicals and non-ionized phenol molecules can be postulated,

$$S{-}^{*}OH + HPh \rightarrow \text{products}$$

where S denotes the surface of the TiO_2 particles. The rate of the oxidation reaction would thus be proportional to the product of the concentrations of hydroxyl radical and non-ionized phenol molecular:

$$r \propto [S{-}^{*}OH][HPh]$$

The hydroxyl radicals stem largely from the reaction between light-excited holes (h^+) and surface hydroxyl groups [37],

$$h^+ + S{-}OH^- \rightarrow S{-}^{*}OH$$

Thus the concentration of the hydroxyl radicals depends on the concentration of surface hydroxyl groups, which are in turn determined by the dissociation of hydrous TiO_2,

$$S\text{-}OH_2 \underset{K_2}{\overset{K_1}{\rightleftharpoons}} \begin{matrix} S\text{-}OH^- + H^+ \\ S\text{-}H^+ + OH^- \end{matrix}$$

Consequently, the concentration of hydroxyl radicals is related to H^+ concentration,

$$[S{-}^{*}OH] \propto \frac{K_1 K_w}{K_1 K_w + [H^+]K_w + [H^+]^2 K_2}$$

where K_w is the equilibrium constant for water dissociation.

According to the dissociation of phenol,

$$HPh \overset{K_a}{\rightleftharpoons} H^+ + Ph^- \qquad pK_a = 9.89$$

the concentration of non-ionized phenol molecular is also related to H^+ concentration,

$$[HPh] \propto \frac{[H^+]}{[H^+] + K_a}$$

Thus the rate depends on H^+ concentration as,

$$r \propto \left\{\frac{K_1 K_w}{K_1 K_w + [H^+]K_w + [H^+]^2 K_2}\right\}\left\{\frac{[H^+]}{[H^+] + K_a}\right\}$$

Both constants K_1 and K_2 are uncertain but pK_1 and pK_2 are believed to be near to the isoelectric point of TiO_2 and follow the rule [53],

$$IEP_{TiO_2} = \frac{pK_1 + pK_2}{2}$$

The IEP_{TiO_2} is reported varying from 4.0 to 6.8 [12,40,54]. Holding $pK_1 = 5.0$ and $pK_2 = 7.0$ (i.e., assuming $IEP_{TiO_2} = 6.0$), the r–pH correlation is then shown as the dotted line in Fig. 8, which fit well the experimental observations though there is a slight discrepancy between the experimental curve and the fitting curve, i.e., a shift along the pH axis between two curves.

3.5. Reuse of the particles

The reusability of the magnetic photocatalysts is shown in Fig. 9. The phenol removal efficiencies of the catalyst over seven uses (only Ti/Si/BS-A was evaluated) give an average value of ~7.0 wt%, slightly down compared to that of the first use (8.0 wt%). The change of the contents of Fe, Si and Ti after repeated use is not significant until after six uses (indicated by SEM–EDS analysis in Table 1). After eight uses, both Si and Ti percentages decreased while that of iron increased. The particles were repeatedly used for more than 50 h (effectively 50 runs of 1 h duration) in this research and the phenol removal efficiency finally became ~5.0 wt%. The

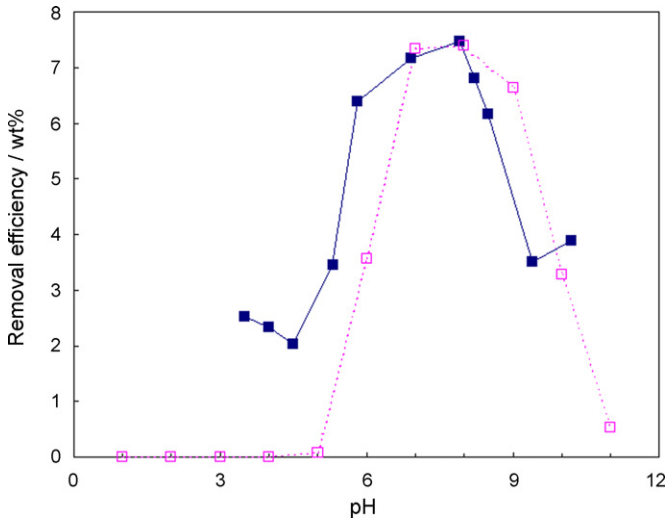

Fig. 8. pH dependence of the phenol removal efficiency after 1-h photoreaction. Solid square: observations; open square: fitted points.

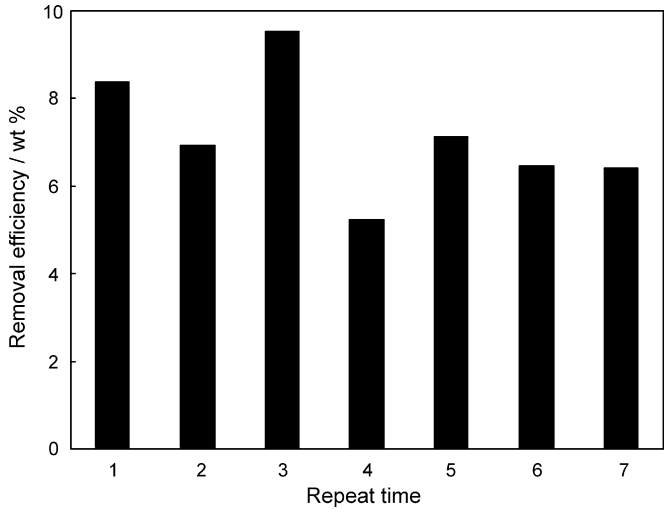

Fig. 9. The phenol removal efficiency after 1-h photoreaction achieved by the repeat uses of the Ti/Si/BS-A photocatalysts.

decrease in reactivity is probably a result of the loss of the photoreactive component TiO_2 via the following two processes: (a) the surface TiO_2 components are dislodged by stirring and lost from the Si/BS particle, thus becoming unrecoverable with the magnetic bar, and (b) the aggregates of Ti/Si/BS are fragmented by stirring and transformed to individual particles that are too small to be magnetically recoverable. The latter scenario would be rectified with a stronger magnetic field.

4. Conclusions

A natural magnetic material, black sand, was used as a core to prepare a magnetic photocatalyst, which is easily recoverable using an external magnetic field. A surfactant mediated scheme was used to deposit a rough silica layer on the surface of black sand, which otherwise could not be coated with silica through the conventional scheme using Stöber process. Titanium dioxide was deposited on the surface of Si/BS composite through both an impregnation process and a direct deposition process. The latter is preferred as it avoided the calcination process to obtain anatase TiO_2. The resultant photocatalyst (Ti/Si/BS) exhibited a lower reactivity than Degussa P25 TiO_2. This was attributed to a smaller amount of TiO_2 deposited on the Ti/Si/BS photocatalyst. The oxidation rate showed a pH dependence, which was ascribed to (a) pH effect on the formation of $^{\bullet}OH$ and (b) pH effect on the electrostatic interaction between the photocatalyst and the substrate. The prepared photocatalyst is reusable despite slight deactivation caused by the mechanical loss of TiO_2. As far as the practical application is concerned, the development of the Ti/Si/BS photocatalyst envisages the use of other coarse materials (e.g., iron filing) as magnetic cores that are economically and technically favorable.

Acknowledgement

This work was financed by the joint scholarship between University of East Anglia and Chinese Scholarship Council. The authors also thank Prof. Maochu Gong of Institute of Catalyst Research, Sichuan University, for his help with the analysis of surface area.

References

[1] A. Fujishima, X. Zhang, C.R. Chim. 9 (2006) 750–760.
[2] A. Fujishima, K. Honda, Nature 238 (1972) 37.
[3] D.R. Acosta, A.I. Martinez, A.A. Lopez, C.R. Magana, J. Mol. Catal. A 228 (2005) 183–188.
[4] R. Fretwell, P. Douglas, J. Photochem. Photobiol. A 143 (2001) 229–240.
[5] A. Mills, G. Hill, S. Bhopal, I.P. Parkin, S.A. O'Neill, J. Photochem. Photobiol. A 160 (2003) 185–194.
[6] T. Wang, H. Wang, P. Xu, X. Zhao, Y. Liu, S. Chao, Thin Solid Films 334 (1998) 103–108.
[7] R.W. Matthews, Water Res. 24 (1990) 653–660.
[8] W. Fu, H. Yang, L. Chang, H Bala, M. Li, G. Zou, Colloids Surf. A 289 (2006) 47–52.
[9] S.-W. Lee, J. Drwiega, D. Mazyck, C.-Y. Wu, W.M. Sigmund, Mater. Chem. Phys. 96 (2006) 483–488.
[10] D.G. Shchukin, E.A. Ustinovich, D.V. Sviridov, A.I. Kulak, High Energy Chem. 38 (2004) 167–173.
[11] S. Watson, D. Beydoun, R. Amal, J. Photochem. Photobiol. A 148 (2002) 303–313.
[12] S. Watson, J. Scott, D. Beydoun, R. Amal, J. Nanopart. Res. 7 (2005) 691–705.
[13] D. Beydoun, R. Amal, G.K.-C. Low, S. McEvoy, J. Phys. Chem. B 104 (2000) 4387–4396.
[14] D. Beydoun, R. Amal, G. Low, S. McEvoy, J. Mol. Catal. A 180 (2002) 193–200.
[15] S. Kurinobu, K. Tsurusaki, Y. Natui, M. Kimata, M. Hasegawa, J. Magn. Magn. Mater. 310 (2007) e1025–e1027.
[16] W. Qiu, Y. Zheng, K.A. Haralampides, Chem. Eng. J. 125 (2007) 165–176.
[17] A. Jitianu, M. Raileanu, M. Crisan, D. Predoi, M. Jitianu, L. Stanciu, M. Zaharescu, J. Sol-Gel Sci. Technol. 40 (2006) 317–323.
[18] P. Wu, J. Zhu, Z. Xu, Adv. Funct. Mater. 14 (2004) 345–351.
[19] D. Bahnemann, A. Henglein, J. Lilie, L. Spanhel, J. Phys. Chem. 88 (1984) 709–711.
[20] S.w. Lee, J. Drwiega, C.Y. Wu, D. Mazyck, W.M. Sigmund, Chem. Mater. 16 (2004) 1160–1164.
[21] M. Ettinger, C. Ruchhoft, R. Lishka, Anal. Chem. 23 (1951) 1783–1788.
[22] G. Sivalingam, M.H. Priya, G. Madras, Appl. Catal. B 51 (2004) 67–76.
[23] V.V. Serdobintseva, D.V. Kalinin, A.F. Danilyuk, A.I. Plehanov, D.A. Kurdyukov, N.A. Rudina, React. Kinet. Catal. Lett. 84 (2005) 389–394.
[24] N.Z. Rao, L.D. Gelb, J. Phys. Chem. B 108 (2004) 12418–12428.
[25] T.T. Trinh, A.P.J. Jansen, R.A. Van Santen, J. Phys. Chem. B 110 (2006) 23099–23106.
[26] M.-S. Tsai, P.Y. Huang, C.-H. Yang, J. Nanopart. Res. 8 (2006) 943–949.
[27] A.P.R. Johnston, B.J. Battersby, G.A. Lawrie, L.K. Lambert, M. Trau, Chem. Mater. 18 (2006) 6163–6169.
[28] W. Stöber, A. Fink, E. bohn, J. Colloid Interf. Sci. 26 (1968) 62–69.
[29] S.-L. Chen, P. Dong, G.-H. Yang, J.-J. Yang, Ind. Eng. Chem. Res. 35 (1996) 4487–4493.
[30] A.G. Howard, N.H. Khdary, Mater. Lett. 61 (2007) 1951–1954.
[31] C.T. Kresge, M.E. Leonowicz, W.J. Roth, J.C. Vartuli, J.S. Beck, Nature 359 (1992) 710–712.
[32] J.S. Beck, J.C. Vartuli, W.J. Roth, M.E. Leonowicz, C.T. Kresge, K.D. Schmitt, C.T.W. Chu, D.H. Olson, E.W. Sheppard, S.B. McCullen, J.B. Higgins, J.L. Schlenker, J. Am. Chem. Soc. 114 (1992) 10834–10843.
[33] I. Pastoriza-Santos, J. Perez-Juste, L.M. Liz-Marzan, Chem. Mater. 18 (2006) 2465–2467.
[34] M. Ogawa, N. Shimura, A. Ayral, Chem. Mater. 18 (2006) 1715–1718.
[35] L. Zhao, J. Yu, J. Colloid Interf. Sci. 304 (2006) 84–91.
[36] R. Kun, K. Mogyorosi, I. Dekany, Appl. Clay Sci. 32 (2006) 99–110.
[37] K. Chhor, J.F. Bocquet, C. Colbeau-Justin, Mater. Chem. Phys. 86 (2004) 123–131.

[38] T. Alapi, P. Sipos, I. Ilisz, G. Wittmann, Z. Ambrus, I. Kiricsi, K. Mogyorosi, A. Dombi, Appl. Catal. A 303 (2006) 1–8.
[39] M. Gopal, W.J.M. Chan, L.C.D. Jonghe, J. Mater. Sci. V32 (1997) 6001–6008.
[40] W.K. Choy, W. Chu, Ind. Eng. Chem. Res. (2005) 8184–8189.
[41] D. Vione, C. Minero, V. Maurino, M.E. Carlotti, T. Picatonotto, E. Pelizzetti, Appl. Catal. B 58 (2005) 81–90.
[42] Y. Chen, K. Wang, L. Lou, J. Photochem. Photobiol. A 163 (2004) 281–287.
[43] K.Y. Jung, S.B. Park, S.-K. Ihm, Appl. Catal. A 224 (2002) 229–237.
[44] G. Sivalingam, K. Nagaveni, M.S. Hegde, G. Madras, Appl. Catal. B 45 (2003) 23–38.
[45] B. Bai, J. Zhao, X. Feng, Mater. Lett. 57 (2003) 3914–3918.
[46] H. Chun, W. Yizhong, T. Hongxiao, Appl. Catal. B 30 (2001) 277–285.
[47] G.S. Shephard, S. Stockenstrom, D. de Villiers, W.J. Engelbrecht, G.F.S. Wessels, Water Res. 36 (2002) 140–146.
[48] S.-X. Li, F.-Y. Zheng, X.-l. Liu, F. Wu, N.-S. Deng, J.-H. Yang, Chemosphere 61 (2005) 589–594.
[49] I. Othman, R.M. Mohamed, F.M. Ibrahem, J. Photochem. Photobiol. A 189 (2007) 80–85.
[50] R.M. Mohamed, A.A. Ismail, I. Othman, I.A. Ibrahim, J. Mol. Catal. A 238 (2005) 151–157.
[51] C.-H. Wu, Chemosphere 57 (2004) 601–608.
[52] C.-N. Chang, Y.-S. Ma, G.-C. Fang, A.C. Chao, M.-C. Tsai, H.-F. Sung, Chemosphere 56 (2004) 1011–1017.
[53] W. Stumm, Chemistry of the Solid-water Interface, John Wiley & Sons, Inc., New York, 1992, p. 20.
[54] W.-Y. Wang, Y. Ku, Colloids Surf. A 302 (2007) 261–268.